JOURNAL OF SPACECRAFT AND ROCKETS
Vol. 38, No. 6, November–December 2001

# Multigrid Algorithm for Computing Hypersonic, Chemically Reacting Flows

Sung-soo Kim,* Chongam Kim,† and Oh-Hyun Rho‡
*Seoul National University, Seoul 151-742, Republic of Korea*

**A robust and efficient multigrid method for computing inviscid and viscous high-speed steady-state reactive flows is presented. Curve-fitted data are used to calculate equilibrium properties. Nonequilibrium flows are calculated using five-species and two-temperature air models. The advection upstream splitting method by pressure-based weight functions is used to acquire robustness and spatial accuracy in capturing a shock and resolving a boundary layer. The five-stage Runge–Kutta and lower-upper symmetric Gauss–Seidel schemes are adopted for efficient time integration. The chemical source terms are treated in a point-implicit manner when five-stage Runge–Kutta is used. To overcome the stability problem in applying the multigrid method to high-speed reactive flow calculations, a modified damped prolongation and a new implicit residual smoothing are proposed. The proposed methods are applied to the computations of hypersonic equilibrium and nonequilibrium flows over a half-cylinder. The results reveal the robustness of the proposed methods and substantial multigrid speed-ups in both the equilibrium and nonequilibrium test cases.**

## Nomenclature

| | | |
|---|---|---|
| $\boldsymbol{A}, \boldsymbol{B}$ | = | flux Jacobian matrices |
| $a$ | = | speed of sound, m/s |
| $e, e_t, h$ | = | internal energy, total energy, enthalpy per unit mass, J/kg |
| $M$ | = | Mach number or molecular weight |
| $p$ | = | pressure, N/m$^2$ |
| $T$ | = | temperature, K |
| $t$ | = | time, s |
| $u, v$ | = | velocity components in the $x$ and $y$ directions, m/s |

*Subscripts*

| | | |
|---|---|---|
| $i$ or $s$ | = | species |
| rot | = | rotational |
| trans | = | translational |
| $v$ or vib | = | vibrational |

## Introduction

AS a means of realizing a high-speed transportation system for the 21st century, the engineering analysis and design of hypersonic flight vehicles have emerged as an important research field. Numerous studies are carried out to unveil the physics of hypersonic flows experimentally or numerically. Computations of hypersonic flows using computational fluid dynamics, however, suffer from a very slow convergence toward a steady state, leading to high computational cost and inefficient numerical analysis. One of the main reasons is the broad spectrum of the Mach number in the flowfields, which results in very different timescales. Another is the chemical reaction in high-temperature regions. The ratio between fluid dynamic timescale associated with convection, diffusion, and chemical reaction timescale can be higher than $10^6$, which makes it very difficult for numerical solutions to converge to steady states. Highly nonlinear behavior near strong shock regions also deteriorates the convergence rate. Thus, the need for efficient numerical techniques to solve the governing equations of hypersonic chemically reacting flows has become very obvious over the past few years. Although the multigrid method has been successfully applied to subsonic and transonic flow calculations, yielding a significant increase in the convergence rate, the application of the multigrid method to hypersonic reactive flows is still limited because of unphysical negative density and/or pressure near a strong shock or expansion region. This robustness problem is considered to be one of the main threats in the application of the multigrid method to hypersonic flow computations.

Several studies have been carried out to improve the performance of the multigrid in high-speed flows. Turkel et al.[1] calculate hypersonic viscous two- and three-dimensional flows using the multigrid method with an explicit Runge–Kutta scheme. A full multigrid (FMG) method is used to provide a well-conditioned starting solution for fine grids. To avoid numerical difficulties associated with freestream conditions, they start the calculation with a lower Mach number and gradually increase the Mach number to the desired flow conditions. A numerical dissipation, which is shown to be the crucial aspect of their multigrid method, is formulated to overcome instability near a shock and to preserve a good shock-capturing property. Also, variable coefficients in the implicit residual smoothing are introduced to remove the diffusion limit on the time step, and constant coefficients implicit residual smoothing is applied to the coarse grid corrections being transferred to fine grids. This process acts to reduce unphysical upstream influence and high-frequency oscillations, which are caused by standard prolongation near strong shocks and make multigrid unstable in hypersonic flows.

The central restriction operator used in the standard multigrid algorithm for subsonic and transonic flow regimes allows unphysical upstream propagation of disturbances in the case of supersonic and hypersonic flows. To cure such phenomena, a pressure-based damping of restricted residual is widely used. For inviscid hypersonic flows Koren and Hemker[2] show that the local damping of restricted residual improves the robustness of the multigrid method. Radespiel and Swanson[3] also use a damped restriction for the same purpose. A pressure-based switch is exploited to detect strong shocks and to damp restricted residual near-shock regions, which is in line with the restriction damping technique of Koren and Hemker.[2]

The damped method can be applied to the prolongation and the time step. Gerlinger et al.[4] design a hybrid switch using a standard pressure-based sensor and a sensor with total variation diminishing properties to detect strong shocks and use it to damp restricted residual, prolongated correction and the time step.[4–6] Edwards[7] uses a Frechét derivative approximation to treat residual error and successfully calculates chemically reacting viscous flows using the

Presented as Paper 2000-2479 at the Fluids 2000 Conference, Denver, CO, 19–22 June 2000; received 30 August 2000; revision received 12 May 2001; accepted for publication 19 May 2001. 

*Graduate Student, Department of Aerospace Engineering.
†Assistant Professor, Department of Aerospace Engineering. Member AIAA.
‡Professor, Department of Aerospace Engineering. Senior Member AIAA.

multigrid. In this approximation residual error is calculated as in the linear multigrid method to minimize the influence of the large change in a coarse-grid solution resulting from the combination of strong discontinuities and low resolution. However, the optimal parameter value is not mentioned. Zhu et al.[8] proposed a pressure-based sensor for damped prolongation. This sensor is calculated with pressure values on the fine grid, prolongated from the initial solution on the corresponding coarse grid, and prolongated from the coarse grid solution after a few smoothing sweeps. This damped prolongation is simple and helps to stabilize transient solutions. With the pressure-based damped prolongation two- and three-dimensional hypersonic flows are calculated. However, their applications are limited to frozen flows.

In the present paper a FMG method with damped prolongation is used to calculate hypersonic flows. The damped prolongation proposed in Ref. 8 is modified to a simpler form based on numerical analysis, and test cases are extended to hypersonic reactive flows including equilibrium inviscid, viscous flows, and nonequilibrium inviscid, viscous flows. The results show that the modified damped prolongation helps to stabilize transient solutions of the multigrid method. For smoothing sweeps lower-upper symmetric Gauss–Seidel (LU-SGS) and five-stage Runge–Kutta schemes associated with an implicit residual smoothing are used. Based on the stability analysis of a convection-diffusion equation, new variable coefficients for the implicit residual smoothing are developed, which enhance local stability significantly. These new variable coefficients make the multigrid procedure more stable and help to acquire a very good convergence rate. When nonequilibrium flow is calculated with the five-stage Runge–Kutta scheme, the chemical reaction source term is treated point implicitly to overcome the time-step restriction. Comparisons in multigrid efficiency between the five-stage Runge–Kutta and the LU-SGS time integration are presented.

## Governing Equations

**Equilibrium Flow**

When the density is sufficiently high so that there are enough collisions between particles to allow the equilibration of energy transfer between the various modes, the flow is in equilibrium. For equilibrium flow any two thermodynamic properties can be used to define the state of flow uniquely. The governing equations for equilibrium laminar viscous flows in a nondimensionalized conservation form can be written as

$$\frac{\partial \boldsymbol{Q}}{\partial t}+\frac{\partial \boldsymbol{E}}{\partial x}+\frac{\partial \boldsymbol{F}}{\partial y}=\left(\frac{\partial \boldsymbol{E}_v}{\partial x}+\frac{\partial \boldsymbol{F}_v}{\partial y}\right) \tag{1}$$

where

$$\boldsymbol{Q}=\begin{bmatrix}\rho\\ \rho u\\ \rho v\\ \rho e_t\end{bmatrix},\qquad \boldsymbol{E}=\begin{bmatrix}\rho u\\ \rho u^2+p\\ \rho uv\\ (\rho e_t+p)u\end{bmatrix},\qquad \boldsymbol{F}=\begin{bmatrix}\rho v\\ \rho vu\\ \rho v^2+p\\ (\rho e_t+p)v\end{bmatrix}$$

$$\boldsymbol{E}_v=\frac{1}{Re_c}\begin{bmatrix}0\\ \tau_{xx}\\ \tau_{xy}\\ e_v\end{bmatrix},\qquad \boldsymbol{F}_v=\frac{1}{Re_c}\begin{bmatrix}0\\ \tau_{xy}\\ \tau_{yy}\\ f_v\end{bmatrix} \tag{2}$$

with $e_v=u\tau_{xx}+v\tau_{xy}-q_x$, $f_v=u\tau_{xy}+v\tau_{yy}-q_y$, $Re_c=\rho_\infty c_\infty L/\mu_\infty$.

The equation of state is

$$p=(\tilde{\gamma}-1)\rho e=(\tilde{\gamma}-1)\rho\left[e_t-\tfrac{1}{2}(u^2+v^2)\right] \tag{3}$$

The specific heat ratio $\tilde{\gamma}$ in Eq. (3) is the function of two thermodynamic variables. In the present paper thermodynamic properties such as pressure and temperature in equilibrium state are calculated using curve-fitted data.[9] Transport properties such as viscosity and conductivity are also calculated using curve-fitted data.[10]

**Nonequilibrium Flow**

The dynamic behavior of a flow is significantly affected by chemical reactions when a nonequilibrium reacting flow is computed. Therefore, all of the species and vibrational energies of molecules should be added to the governing equations as additional flow variables. In the present paper a five-species two-temperature air model[11–13] is used in the temperature range of 2500 K $< T <$ 9000 K. For the reaction rate constant Blottner's model[14] is adopted:

$$\begin{gathered}\mathrm{O_2}+M\leftrightarrow \mathrm{O}+\mathrm{O}+M,\qquad \mathrm{N_2}+M\leftrightarrow N+N+M\\ \mathrm{NO}+M\leftrightarrow N+\mathrm{O}+M,\qquad \mathrm{O}+\mathrm{NO}\leftrightarrow N+\mathrm{O_2}\\ \mathrm{O}+\mathrm{N_2}\leftrightarrow N+\mathrm{NO}\end{gathered} \tag{4}$$

where $M$ can be any one of the five possible collision partners.

The governing equations for nonequilibrium laminar viscous flows in a nondimensionalized conservation form are written as

$$\frac{\partial \boldsymbol{Q}}{\partial t}+\frac{\partial \boldsymbol{E}}{\partial x}+\frac{\partial \boldsymbol{F}}{\partial y}=\left(\frac{\partial \boldsymbol{E}_v}{\partial x}+\frac{\partial \boldsymbol{F}_v}{\partial y}\right)+\boldsymbol{S} \tag{5}$$

where

$$\boldsymbol{Q}=\begin{bmatrix}\rho\\ \rho u\\ \rho v\\ \rho e_t\\ \rho_1\\ \rho_2\\ \rho_3\\ \rho e_{\mathrm{vib}}\end{bmatrix},\qquad \boldsymbol{E}=\begin{bmatrix}\rho u\\ \rho u^2+p\\ \rho uv\\ (\rho e_t+p)u\\ \rho_1 u\\ \rho_2 u\\ \rho_3 u\\ \rho e_{\mathrm{vib}}u\end{bmatrix}$$

$$\boldsymbol{F}=\begin{bmatrix}\rho v\\ \rho vu\\ \rho v^2+p\\ (\rho e_t+p)v\\ \rho_1 v\\ \rho_2 v\\ \rho_3 v\\ \rho e_{\mathrm{vib}}v\end{bmatrix},\qquad \boldsymbol{E}_v=\begin{bmatrix}0\\ \tau_{xx}\\ \tau_{xy}\\ e_v\\ \rho D_1\dfrac{\partial c_1}{\partial x}\\ \rho D_2\dfrac{\partial c_2}{\partial x}\\ \rho D_3\dfrac{\partial c_3}{\partial x}\\ E_{\mathrm{vib}}\end{bmatrix}$$

$$\boldsymbol{F}_v=\begin{bmatrix}0\\ \tau_{xy}\\ \tau_{yy}\\ f_v\\ \rho D_1\dfrac{\partial c_1}{\partial y}\\ \rho D_2\dfrac{\partial c_2}{\partial y}\\ \rho D_3\dfrac{\partial c_3}{\partial y}\\ F_{\mathrm{vib}}\end{bmatrix},\qquad \boldsymbol{S}=\begin{bmatrix}0\\ 0\\ 0\\ 0\\ \dot{w}_1\\ \dot{w}_2\\ \dot{w}_3\\ \sum_{s=1}^{3}\rho_s\dot{e}_{\mathrm{vib},s}+\dot{w}_s e_{\mathrm{vib},s}\end{bmatrix} \tag{6}$$

with

$$e_v=u\tau_{xx}+v\tau_{xy}-\left(q_x+\sum_{s=1}^{3}q_{vx,s}\right)+\sum_{s=1}^{5}\left(\rho_s h_s D_s\frac{\partial c_s}{\partial x}\right)$$

$$f_v=u\tau_{xy}+v\tau_{yy}-\left(q_y+\sum_{s=1}^{3}q_{vy,s}\right)+\sum_{s=1}^{5}\left(\rho_s h_s D_s\frac{\partial c_s}{\partial y}\right)$$

$$E_{\text{vib}} = \sum_{s=1}^{3} \rho e_{\text{vib},s} D_s \frac{\partial c_s}{\partial x} - q_{vx,s}$$

$$F_{\text{vib}} = \sum_{s=1}^{3} \rho e_{\text{vib},s} D_s \frac{\partial c_s}{\partial y} - q_{vy,s}$$

$$q_{vx,s} = -\kappa_{\text{vib},s} \frac{\partial T_{\text{vib}}}{\partial x}, \qquad q_{vy,s} = -\kappa_{\text{vib},s} \frac{\partial T_{\text{vib}}}{\partial y}$$

$$c_s = \frac{\rho_s}{\rho} \text{ (mass fraction)}$$

The viscosity model of Blottner et al.[14] is used to calculate the species viscosity $\mu_i$:

$$\mu_i = 0.1 \exp[(A_i \ln T + B_i) \ln T + C_i] \tag{7}$$

where $A_i$, $B_i$, and $C_i$ are given in Ref. 14.

The conductivities of the species, which are derived from the Eucken relation,[11] are

$$\kappa_i = \mu_i \left(\tfrac{5}{2} c_{v,\text{tans},i} + c_{v,\text{rot},i}\right), \qquad \kappa_{\text{vib},i} = \mu_i c_{v,\text{vib},i} \tag{8}$$

The diffusion coefficients are computed by

$$D_i = (M_i/M)[(1 - c_i)/(1 - X_i)]D \tag{9}$$

where $D = \mu/\rho Sc$ and $Sc$ is the Schmidt number and is constant.

The total viscosity and conductivity are calculated using Wilke's semi-empirical mixing rule[15]:

$$\mu = \sum_s \frac{\mu_s X_s}{\phi_s}, \qquad \kappa = \sum_s \frac{\kappa_s X_s}{\phi_s} \tag{10}$$

where

$$X_i = \frac{c_i M}{M_i}, \qquad M = \left(\sum_s \frac{c_s}{M_s}\right)^{-1}$$

$$\phi_i = \sum_s X_s \left[1 + \sqrt{\frac{\mu_i}{\mu_s}} \left(\frac{M_s}{M_i}\right)^{\frac{1}{4}}\right]^2 \left[\sqrt{8\left(1 + \frac{M_i}{M_s}\right)}\right]^{-1}$$

Vector $\boldsymbol{S}$ represents the source term for thermochemical phenomena, which includes the source of the species, $\dot{w}_s$ in the species continuity equations and $(\rho_s \dot{e}_{\text{vib},s} + \dot{w}_s e_{\text{vib},s})$ in the vibrational energy equation. The species equations for $O_2$ and $N_2$ (for $\rho_4$ and $\rho_5$) are excluded in the governing equations to reduce the computational time and memory storage. The density values of $O_2$ and $N_2$ are obtained from the global mass conservation equation and the elemental conservation condition between oxygen and nitrogen.[16]

The equation of state is

$$p = \sum_s \rho_s \frac{\boldsymbol{R}}{M_s} T \tag{11}$$

where $\boldsymbol{R}$ is the universal gas constant (8.314 kJ/kg · mole · K) and $M_s$ is the molecular weight of each species in nonequilibrium gas.

## Space Discretization

The advection upstream splitting method by pressure-based weight functions (AUSMPW)[17] scheme is used for space discretization. The main feature of AUSMPW is to remove oscillations of AUSM+[18] near a wall or across a strong shock while maintaining the accuracy of the original scheme. The numerical flux of AUSMPW is written as follows:

$$\boldsymbol{F}_{\frac{1}{2}} = \bar{M}_L^+ c_{\frac{1}{2}} \boldsymbol{\Phi}_L + \bar{M}_R^- c_{\frac{1}{2}} \boldsymbol{\Phi}_R + \left(P_L^+\big|_{\alpha=\frac{3}{16}} \boldsymbol{P}_L + P_R^-\big|_{\alpha=\frac{3}{16}} \boldsymbol{P}_R\right) \tag{12}$$

where

$$m_{\frac{1}{2}} = M_L^+\big|_{\beta=\frac{1}{8}} + M_R^-\big|_{\beta=\frac{1}{8}}$$

1) $m_{\frac{1}{2}} \geq 0$:

$$\bar{M}_L^+ = M_L^+\big|_{\beta=\frac{1}{8}} + M_R^-\big|_{\beta=\frac{1}{8}} + M_R^-\big|_{\beta=\frac{1}{8}} \times w \cdot (1 + f_R) + \left(f_L M_L^+\big|_{\beta=\frac{1}{8}} + f_R M_R^-\big|_{\beta=\frac{1}{8}}\right)$$

$$\bar{M}_R^- = M_R^-\big|_{\beta=\frac{1}{8}} \times w \cdot (1 + f_R)$$

2) $m_{\frac{1}{2}} < 0$:

$$\bar{M}_L^+ = M_L^+\big|_{\beta=\frac{1}{8}} \times w \cdot (1 + f_L)$$

$$\bar{M}_R^- = M_L^+\big|_{\beta=\frac{1}{8}} + M_R^-\big|_{\beta=\frac{1}{8}} + M_L^+\big|_{\beta=\frac{1}{8}} \times w \cdot (1 + f_L) + \left(f_L M_L^+\big|_{\beta=\frac{1}{8}} + f_R M_R^-\big|_{\beta=\frac{1}{8}}\right)$$

and $\boldsymbol{\Phi} = (\rho, \rho u, \rho H)^T$, $\boldsymbol{P} = (0, p, 0)^T$.

$f_{L,R}$ and pressure-based weight function $w$ are as follows:

$$f_{L,R} = \begin{cases} \left(\dfrac{p_{L,R}}{p_s} - 1\right) pl(p_{L,R}, p_{R,L}) \times \left|M_{L,R}^{\pm}\big|_{\beta=0}\right| \\ \qquad \times \min\left[1, \left(\dfrac{|\boldsymbol{V}_{L,R}|}{c_{\frac{1}{2}}}\right)^{0.25}\right], & |M_{L,R}| \leq 1 \\ 0, & |M_{L,R}| > 1 \end{cases} \tag{13}$$

$$w(p_L, p_R) = 1 - \min\left(\frac{p_L}{p_R}, \frac{p_R}{p_L}\right)^3 \tag{14}$$

where

$$pl(x, y) = \begin{cases} 4 \cdot \min\left(\dfrac{x}{y}, \dfrac{y}{x}\right) - 3, & \dfrac{3}{4} \leq \min\left(\dfrac{x}{y}, \dfrac{y}{x}\right) < 1 \\ 0, & 0 \leq \min\left(\dfrac{x}{y}, \dfrac{y}{x}\right) < \dfrac{3}{4} \end{cases}$$

$$p_s = P_L^+\big|_{\alpha=\frac{3}{16}} p_L + P_R^-\big|_{\alpha=\frac{3}{16}} p_R \tag{15}$$

The split Mach number and the split pressure of AUSMPW at the cell interface are as follows:

$$M^{\pm}\big|_{\beta} = \begin{cases} \pm\frac{1}{4}(M \pm 1)^2 \pm \beta(M^2 - 1)^2 & |M| \leq 1 \\ \frac{1}{2}(M \pm |M|) & |M| > 1 \end{cases} \tag{16}$$

$$p^{\pm}\big|_{\alpha} = \begin{cases} \frac{1}{4}(M \pm 1)^2(2 \mp M) \pm \alpha M(M^2 - 1)^2 & |M| \leq 1 \\ \frac{1}{2}[1 \pm \text{sign}(M)] & |M| > 1 \end{cases} \tag{17}$$

The Mach number of each side is defined as follows:

$$M_{L,R} = U_{L,R} \big/ c_{\frac{1}{2}}, \qquad c_{\frac{1}{2}} = \min(\tilde{c}_L, \tilde{c}_R) \tag{18}$$

where $\tilde{c} = c^{*2} / \max(|U|, c^*)$, $c^* = \sqrt{\{[2(\gamma - 1)/(\gamma + 1)]H\}}$, and $U$ is the contravariant velocity.

## Time Integration

### Explicit Time Integration

The five-stage Runge–Kutta scheme adopted in the present study has the following form:

$$\boldsymbol{Q}^{(0)} = \boldsymbol{Q}^n, \qquad \boldsymbol{Q}^{(k)} = \boldsymbol{Q}^{(0)} - \alpha_k J \Delta t \boldsymbol{R}^{(k-1)}, \qquad \boldsymbol{Q}^{n+1} = \boldsymbol{Q}^{(5)} \tag{19}$$

where

$$\alpha_1 = \frac{1}{4}, \qquad \alpha_2 = \frac{1}{6}, \qquad \alpha_3 = \frac{3}{8}, \qquad \alpha_4 = \frac{1}{2}$$

$$\alpha_5 = 1, \qquad \boldsymbol{R}^{k-1} = \left[ \frac{\partial \hat{\boldsymbol{E}}}{\partial \xi} + \frac{\partial \hat{\boldsymbol{F}}}{\partial \eta} - \left( \frac{\partial \hat{\boldsymbol{E}}_v}{\partial \xi} + \frac{\partial \hat{\boldsymbol{F}}_v}{\partial \eta} \right) - \boldsymbol{S} \right]^{k-1}$$

For nonequilibrium flows, the species production terms obtained from finite rate chemical reactions introduce additional stiffness into the equation set causing the algorithm to be unstable except for very small Courant–Friedrichs–Lewy (CFL) numbers. To overcome the time-step restriction imposed by the chemical source terms, the source terms are evaluated implicitly.[19] A Taylor-series expansion is performed on this term, which is given by

$$(\boldsymbol{I} - \alpha_k J \Delta t \boldsymbol{H}) \left[ \boldsymbol{Q}^{(k)} - \boldsymbol{Q}^{(0)} \right] = -\alpha_k J \Delta t \boldsymbol{R}^{(k-1)} \tag{20}$$

where $\boldsymbol{H} = \partial \boldsymbol{S} / \partial \boldsymbol{Q}$. This is called the point-implicit method because the implicit terms are not spatially differenced but are evaluated point by point.

#### Implicit Time Integration

The governing equations can be discretized using the Euler backward method in time as follows:

$$\left( \boldsymbol{I}/J\Delta t + \delta_\xi^- \hat{\boldsymbol{A}}^+ + \delta_\xi^+ \hat{\boldsymbol{A}}^- + \delta_\eta^- \hat{\boldsymbol{B}}^+ + \delta_\eta^+ \hat{\boldsymbol{B}}^- - \boldsymbol{H} \right)^n \Delta \boldsymbol{Q}_{i,j}^n = -\boldsymbol{R}_{i,j}^n \tag{21}$$

where

$$\Delta \boldsymbol{Q}_{i,j}^n = \boldsymbol{Q}_{i,j}^{n+1} - \boldsymbol{Q}_{i,j}^n, \qquad \hat{\boldsymbol{A}} = \frac{\partial \hat{\boldsymbol{E}}}{\partial \boldsymbol{Q}}, \qquad \hat{\boldsymbol{B}} = \frac{\partial \hat{\boldsymbol{F}}}{\partial \boldsymbol{Q}}$$

The left-hand-side matrix of Eq. (21) is inverted approximately by the LU-SGS scheme as follows:

$$\boldsymbol{L}\boldsymbol{D}^{-1}\boldsymbol{U} \Delta \boldsymbol{Q}_{i,j}^n = -\boldsymbol{R}_{i,j}^n \tag{22}$$

where

$$\boldsymbol{L} = \boldsymbol{I}/J\Delta t + \delta_\xi^- \hat{\boldsymbol{A}}^+ + \delta_\eta^- \hat{\boldsymbol{B}}^+ - \hat{\boldsymbol{A}}^- - \hat{\boldsymbol{B}}^- - \boldsymbol{H}$$

$$\boldsymbol{D} = \boldsymbol{I}/J\Delta t + \hat{\boldsymbol{A}}^+ + \hat{\boldsymbol{B}}^+ - \hat{\boldsymbol{A}}^- - \hat{\boldsymbol{B}}^-$$

$$\boldsymbol{U} = \boldsymbol{I}/J\Delta t + \delta_\xi^+ \hat{\boldsymbol{A}}^- + \delta_\eta^+ \hat{\boldsymbol{B}}^- - \hat{\boldsymbol{A}}^+ - \hat{\boldsymbol{B}}^+$$

$$\hat{\boldsymbol{A}}^\pm = \tfrac{1}{2}\{\hat{\boldsymbol{A}} \pm \kappa \, |\max[\text{eigenvalue}(\hat{\boldsymbol{A}})]|\}$$

## Implicit Residual Smoothing

#### Implicit Residual Smoothing for Inviscid Flow

The implicit residual smoothing has the following form in two dimensions:

$$(1 - \beta_\xi \nabla_\xi \Delta_\xi)(1 - \beta_\eta \nabla_\eta \Delta_\eta) \bar{\boldsymbol{R}}_{i,j} = \boldsymbol{R}_{i,j} \tag{23}$$

where $\boldsymbol{R}_{i,j}$ is the unsmoothed residual and $\bar{\boldsymbol{R}}_{i,j}$ is the smoothed residual. $\nabla\Delta$ indicates the following form of a standard second-difference operator:

$$\nabla_\xi \Delta_\xi \bar{\boldsymbol{R}}_{i,j} = \bar{\boldsymbol{R}}_{i-1,j} - 2\bar{\boldsymbol{R}}_{i,j} + \bar{\boldsymbol{R}}_{i+1,j} \tag{24}$$

and $\beta$ is a smoothing coefficient. From the analysis of a convection equation, variable coefficients $\beta$ can be obtained as follows[1,20,21]:

$$(\beta_c)_\xi = \max\left\{ \frac{1}{4}\left[ \left( \frac{N}{N^*} \frac{1}{1 + \psi r_{\eta\xi}} \right)^2 - 1 \right], 0 \right\}$$

$$(\beta_c)_\eta = \max\left\{ \frac{1}{4}\left[ \left( \frac{N}{N^*} \frac{1}{1 + \psi r_{\eta\xi}^{-1}} \right)^2 - 1 \right], 0 \right\} \tag{25}$$

where $r_{\eta\xi} = \lambda_\eta / \lambda_\xi$, $\lambda_\xi = |u\xi_x + v\xi_y| + c\sqrt{(\xi_x^2 + \xi_y^2)}$ and $\lambda_\eta = |v\eta_y + u\eta_x| + c\sqrt{(\eta_x^2 + \eta_y^2)}$. The quantity $N/N^*$ is the ratio of the CFL number of the smoothed scheme to that of the basic explicit scheme. The implicit residual smoothing of Eqs. (23) and (25) is used for inviscid flow computations with five-stage Runge–Kutta.

#### Implicit Residual Smoothing for Viscous Flow

From the stability analysis of the diffusion equation, the variable coefficient that will remove the diffusion limit on the time step is obtained as in Ref. 21. The form of $\beta$ is

$$(\beta_d)_\eta = \frac{1}{4}\left[ C_1 \frac{(\lambda_d)_\eta}{\lambda_\xi + \lambda_\eta} - 1 \right] \tag{26}$$

or simply

$$(\beta_d)_\eta = \frac{1}{4} \bar{C}_1 \frac{(\lambda_d)_\eta}{\lambda_\xi + \lambda_\eta} \tag{27}$$

where $(\lambda_d)_\eta = (\gamma\mu/Pr\rho)(\eta_x^2 + \eta_y^2)$ and $\bar{C}_1 \approx 1.0$.

The variable coefficient $\beta$ including the effects of convection and diffusion can be calculated as follows:

$$\beta_\eta = \max[(\beta_c)_\eta, (\beta_d)_\eta] \tag{28}$$

However, the coefficient $\beta_\eta$ of Eq. (28) is found to be insufficient to improve the local stability in the present viscous flow calculation, which makes it difficult to obtain the desirable speed-ups that are usually achieved in inviscid flow calculations. Thus, a new implicit residual smoothing coefficient $\beta$ for viscous flows is developed from the stability analysis of a convection-diffusion equation.

#### New Implicit Residual Smoothing

For the scheme to be stable, it is necessary to restrict the time step by taking into account a convection limit as well as a diffusion limit. The actual time step $\Delta t_{\text{act}}$ based on a sufficient condition for stability can be determined as follows:

$$\Delta t_{\text{act}} \le N(\lambda_\xi + \lambda_\eta + 4\lambda_{\text{viscous}})^{-1} \tag{29}$$

where $N$ is the allowable CFL number. The spectral radii $\lambda_\xi$ and $\lambda_\eta$ of the Jacobian matrices $\boldsymbol{A}$ and $\boldsymbol{B}$, multiplied by the transformation Jacobian $\boldsymbol{J}$, are given by

$$\lambda_\xi = |u\xi_x + v\xi_y| + c\sqrt{\xi_x^2 + \xi_y^2}, \qquad \lambda_\eta = |v\eta_y + u\eta_x| + c\sqrt{\eta_x^2 + \eta_y^2} \tag{30}$$

The spectral radius of viscous terms $\lambda_{\text{viscous}}$ for the thin-layer Navier–Stokes equations is given by

$$\lambda_{\text{viscous}} = (\gamma\mu/Pr\rho)\left(\eta_x^2 + \eta_y^2\right) \tag{31}$$

where $\gamma$ is the specific heat ratio and $Pr$ is the Prandtl number.

The implicit residual smoothing has the following form in two dimensions:

$$(1 - \beta_\xi \nabla_\xi \Delta_\xi)(1 - \beta_\eta \nabla_\eta \Delta_\eta) \bar{\boldsymbol{R}}_{i,j} = \boldsymbol{R}_{i,j} \tag{32}$$

To determine the variable smoothing coefficient $\beta$, the following convection-diffusion equation is considered:

$$\frac{\partial w}{\partial t} + a\frac{\partial w}{\partial x} + b\frac{\partial w}{\partial y} = \mu \frac{\partial^2 w}{\partial y^2} \tag{33}$$

Using central difference approximation for the spatial derivatives, a semidiscrete form of Eq. (33) is written as

$$\Delta t \frac{\mathrm{d}w}{\mathrm{d}t} = -\frac{N_\xi}{2}(w_{i+1,j} - w_{i-1,j}) - \frac{N_\eta}{2}(w_{i,j+1} - w_{i,j-1}) + \frac{N_D}{4}(w_{i,j+1} - 2w_{i,j} + w_{i,j-1}) \tag{34}$$

where the Courant numbers are given by

$$N_\xi = \lambda_\xi \Delta t = (a/\Delta x)\Delta t, \qquad N_\eta = \lambda_\eta \Delta t = (b/\Delta y)\Delta t$$

$$N_D = 4\lambda_{\text{viscous}} \Delta t = 4(\mu/\Delta y^2)\Delta t \tag{35}$$

After taking the discrete Fourier transform of Eq. (34), the following form can be obtained:

$$\Delta t \frac{\mathrm{d}\hat{w}}{\mathrm{d}t} = z\hat{w} \tag{36}$$

where the Fourier symbol is given by

$$z = -i(N_\xi \sin\theta_\xi + N_\eta \sin\theta_\eta) - (N_D/2)\sin^2(\theta_\eta/2) \tag{37}$$

The caret indicates a transformed quantity, and $\theta_\xi$ and $\theta_\eta$ are Fourier angles in the two coordinate directions. If implicit residual smoothing is applied, the Fourier symbol is replaced by

$$z = \frac{-i(N_\xi \sin\theta_\xi + N_\eta \sin\theta_\eta) - (N_D/2)\sin^2(\theta_\eta/2)}{[1 + 2\beta_\xi(1-\cos\theta_\xi)][1 + 2\beta_\eta(1-\cos\theta_\eta)]} \tag{38}$$

Then, a sufficient condition for stability can be written as

$$\max|z| \le N^* \qquad \text{for all} \qquad \theta_\xi \quad \text{and} \quad \theta_\eta \tag{39}$$

where $N^*$ is the CFL number of the unsmoothed scheme. Because

$$|z| = \left| \frac{-i(N_\xi \sin\theta_\xi + N_\eta \sin\theta_\eta) - (N_D/2)\sin^2(\theta_\eta/2)}{[1 + 2\beta_\xi(1-\cos\theta_\xi)][1 + 2\beta_\eta(1-\cos\theta_\eta)]} \right| \tag{40}$$

$$|z| \le \left| \frac{N_\xi \sin\theta_\xi}{[1 + 2\beta_\xi(1-\cos\theta_\xi)]} \right| + \left| \frac{N_\eta \sin\theta_\eta}{[1 + 2\beta_\eta(1-\cos\theta_\eta)]} \right| + \left| \frac{(N_D/2)\sin^2(\theta_\eta/2)}{[1 + 2\beta_\eta(1-\cos\theta_\eta)]} \right| \tag{41}$$

or

$$\max|z| \le N_\xi f(\theta_\xi)_{\max} + N_\eta g(\theta_\eta)_{\max} + N_D h(\theta_\eta)_{\max} \tag{42}$$

a sufficient condition for stability is given by

$$N_\xi f(\theta_\xi)_{\max} + N_\eta g(\theta_\eta)_{\max} + N_D h(\theta_\eta)_{\max} \le N^* \tag{43}$$

with

$$f_{\max} = 1\Big/\sqrt{1+4\beta_\xi}, \qquad g_{\max} = 1\Big/\sqrt{1+4\beta_\eta}$$

$$h_{\max} = 1/(1+4\beta_\eta) \tag{44}$$

Substituting Eq. (44) into Eq. (43) yields

$$N_\xi\left(1\Big/\sqrt{1+4\beta_\xi}\right) + N_\eta\left(1\Big/\sqrt{1+4\beta_\eta}\right) + N_D[1/(1+4\beta_\eta)] \le N^* \tag{45}$$

where

$$N_\xi = N\frac{\lambda_\xi}{\lambda_\xi + \lambda_\eta + 4\lambda_D} = N\frac{1}{1 + r_{\eta\xi} + 4r_{D\xi}}$$

$$N_\eta = N\frac{\lambda_\eta}{\lambda_\xi + \lambda_\eta + 4\lambda_D} = N\frac{1}{1 + r_{\eta\xi}^{-1} + 4r_{D\eta}}$$

$$N_D = N\frac{4\lambda_D}{\lambda_\xi + \lambda_\eta + 4\lambda_D} = N\frac{1}{1 + \frac{1}{4}r_{D\xi}^{-1} + \frac{1}{4}r_{D\eta}^{-1}}$$

Thus, Eq. (45) becomes

$$\frac{N}{N^*}\frac{1}{1 + r_{\eta\xi} + 4r_{D\xi}}\frac{1}{\sqrt{1+4\beta_\xi}} + \frac{N}{N^*}\frac{1}{1 + r_{\eta\xi}^{-1} + 4r_{D\eta}}\frac{1}{\sqrt{1+4\beta_\eta}} + \frac{N}{N^*}\frac{1}{1 + \frac{1}{4}r_{D\xi}^{-1} + \frac{1}{4}r_{D\eta}^{-1}}\frac{1}{1+4\beta_\eta} \le 1 \tag{46}$$

In the cases of low-aspect-ratio cells ($r_{\eta\xi} \ll 1$) at the far field and high-aspect-ratiocells in the boundary layer ($r_{\eta\xi} \gg 1, r_{D\eta} \gg 1$), Eq. (46) can be approximated as

$$\frac{N}{N^*}\frac{1}{1 + r_{\eta\xi} + 4r_D\xi}\frac{1}{\sqrt{1+4\beta_\xi}} \le 1$$

$$\frac{N}{N^*}\frac{1}{1 + \frac{1}{4}r_{D\xi}^{-1} + \frac{1}{4}r_{D\eta}^{-1}}\frac{1}{1+4\beta_\eta} \le 1 \tag{47}$$

respectively. Thus, the variable smoothing coefficient in each direction is given by

$$\beta_\xi = \max\left\{\frac{1}{4}\left[\left(\frac{N}{N^*}\frac{1}{1 + r_{\eta\xi} + 4r_{D\xi}}\right)^2 - 1\right], 0\right\}$$

$$\beta_\eta = \max\left[\frac{1}{4}\left(\frac{N}{N^*}\frac{1}{1 + \frac{1}{4}r_{D\xi}^{-1} + \frac{1}{4}r_{D\eta}^{-1}} - 1\right), 0\right] \tag{48}$$

## Multigrid Approach

### Standard Multigrid Algorithm

The present multigrid scheme is a full approximation scheme.[22] Denoting the mesh level by a subscript $h$, the multigrid procedure starts with a time step on the finest mesh $h = 1$. The underlying coarse meshes (three in the present study) are constructed by successively removing each fine grid line in both coordinate directions (full coarsening). Flow variables of fine grids are restricted to coarse grids by area weighting as

$$\boldsymbol{Q}_{h+1}^{(0)} = \sum S_h \boldsymbol{Q}_h \Big/ S_{h+1} \tag{49}$$

where $S_h$ is the cell area of a fine mesh and $S_{h+1}$ is the sum of the area over four cells of a fine mesh.

Solutions on a coarse mesh are then updated as follows: 1) calculate the correction, and update the solution on the fine mesh; 2) restrict flow quantities to the coarse mesh; 3) collect the residual over four cells of the fine mesh, and calculate the residual on the coarse mesh as

$$\boldsymbol{R}_{h+1}^* = \boldsymbol{R}_{h+1}(\boldsymbol{Q}_{h+1}) + \alpha\sum \boldsymbol{R}_h(\boldsymbol{Q}_h) - \boldsymbol{R}_{h+1}\left(\boldsymbol{Q}_{h+1}^{(0)}\right) \tag{50}$$

where

$$\boldsymbol{R}_h(\boldsymbol{Q}_h) = \left\{\frac{\partial\hat{\boldsymbol{E}}(\boldsymbol{Q}_h)}{\partial\xi} + \frac{\partial\hat{\boldsymbol{F}}(\boldsymbol{Q}_h)}{\partial\eta} - \left[\frac{\partial\hat{\boldsymbol{E}}_v(\boldsymbol{Q}_h)}{\partial\xi} + \frac{\partial\hat{\boldsymbol{F}}_v(\boldsymbol{Q}_h)}{\partial\eta}\right] - \boldsymbol{S}(\boldsymbol{Q}_h)\right\}$$

and 4) calculate the correction and update the solution on the coarse mesh. The residual for the next coarser mesh is calculated as

$$\boldsymbol{R}_{h+2}^* = \boldsymbol{R}_{h+2}(\boldsymbol{Q}_{h+2}) + \alpha\sum \boldsymbol{R}_{h+1}^* - \boldsymbol{R}_{h+2}\left(\boldsymbol{Q}_{h+2}^{(0)}\right) \tag{51}$$

The procedure is repeated down to the coarsest mesh, and finally the correction is sent back to the fine mesh by bilinear interpolation. V-cycle is used in the present paper, i.e., one smoothing sweep at each grid level is performed only at the restriction step.

### Damped Prolongation

The multigrid routine described in the preceding section is very efficient in solving the Euler and Navier–Stokes equations for subsonic and transonic flow problems. In the hypersonic flow regime, however, the standard routine is so unstable that a converged solution is not to be obtained. To stabilize a transient multigrid solution, a damped prolongation is proposed in Ref. 8, which can be described as follows.

The standard prolongation can be written in the following form:

$$\tilde{p}_A = p_A + \left(\tilde{p}_A^{CGC} - p_A^{CGC}\right) \tag{52}$$

where $p_A$ is pressure on the fine grid before multigrid cycle and $\tilde{p}_A$ is pressure on the fine grid after multigrid cycle; $p_A^{CGC}$ stands for pressure on the fine grid prolongated from the initial solution on the coarse grid, i.e., the restricted fine grid solution, and $\tilde{p}_A^{CGC}$ stands for pressure prolongated from the coarse grid solution after a few smoothing sweeps. According to the analysis,[8] the value of $\tilde{p}_A$ can be negative if the value of $p_A^{CGC}$ is much greater than that of $\tilde{p}_A^{CGC}$. To avoid negative pressure in the prolongation step, a damped prolongation is proposed as follows[8]:

$$\tilde{p}_A = p_A + \varphi\left(\tilde{p}_A^{CGC} - p_A^{CGC}\right) \tag{53}$$

with $\varphi = p_A / \max\{p_A, \tilde{p}_A^{CGC}, p_A^{CGC}\}$. This limiter $\varphi$ ensures that the updated pressure $\tilde{p}_A$ is always positive. The damped prolongation method proposed in Ref. 8 works well and enhances robustness during the multigrid cycle.

However, it can be thought that there is no reason to include the term $\tilde{p}_A^{CGC}$ in the limiter $\varphi$. If $\tilde{p}_A^{CGC}$ is the largest value, $\tilde{p}_A$ is always positive without the limiter $\varphi$. It thus suffices to include only the $p_A$ and $p_A^{CGC}$ terms. Unfortunately, the limiter with only these two terms fails to avoid negative pressure. According to the experience of the present study, negative pressure might arise when $\tilde{p}_A^{CGC}$ is the largest value, i.e., when pressure is abruptly changed after smoothing sweeps in the coarse grid. In fact, it is thought that the success of the limiter $\varphi$ is as a result of the $\tilde{p}_A^{CGC}$ term. The kinetic energy across a shock wave is not sufficiently reduced in the coarse grid after smoothing sweeps, such as at the postshock position. Thus, sometimes the kinetic energy exceeds the total energy. This phenomenon leads to the reduction of internal energy after the shock wave propagates, and it results in unphysical negative temperature and pressure. Consequently, it is important to know the location of the shock wave during multigrid cycle and to limit the correction value prolongated from the coarse grid. Only the term $\tilde{p}_A^{CGC}$, not $p_A^{CGC}$, can detect the cells where the shock wave is propagated. The difference between $p_A$ and $\tilde{p}_A^{CGC}$ indicates the location of the cells where flow variables are abruptly changed. In the present paper the following form of modified damped prolongation is proposed and used for all test cases:

$$\tilde{\boldsymbol{Q}}_h = \boldsymbol{Q}_h^{(0)} + \varphi I_{h+1}^h \left[\tilde{\boldsymbol{Q}}_{h+1} - \boldsymbol{Q}_{h+1}^{(0)}\right] \tag{54}$$

with $\phi = \min(1, p_A/\tilde{p}_A^{CGC})$. $I_{h+1}^h$ is a bilinear prolongation operator.

## Numerical Results

Test cases involving hypersonic flows over a 1-m-radius, two-dimensional half-cylinder are considered to evaluate the performance of the reacting-gas multigrid solver with the modified damped prolongation and new implicit residual smoothing. Two $65 \times 113$ grids, one uniformly spaced in the radial direction for the Euler calculations and the other clustered to the cylinder surface for the Navier–Stokes calculations, are considered. All computations are initialized by fixing the freestream fluid properties in the interior of the computational domain. The adiabatic and noncatalytic condition is used for the wall boundary of viscous flows. To check convergence behavior, the $L2$ norm of the discretized fine grid density residual is plotted vs iteration number, which is normalized with respect to the first iteration value. Attempts to obtain a converged solution, with the standard multigrid method disregarding the damped prolongation step, failed for all test cases.

### Equilibrium Inviscid Flow Calculations

Flow conditions correspond to a Mach number 10 flight at an altitude of 60 km. Figure 1 shows the pressure contour and shock profiles along the stagnation streamline, which show monotonic behavior. Both the single-grid and four-level multigrid calculations converged to the level of six orders of magnitude in density residual. No difference can be observed between the single-grid and the four-level multigrid solution.

The single-grid calculation using five-stage Runge–Kutta time integration converged six orders of magnitude in 8848 iterations. The four-level multigrid calculation with the modified damped prolongation of Eq. (54) takes only 710 iterations to achieve the same level of convergence, which is equivalent to a 7.8 speed-up in terms of computational time. The four-level multigrid using five-stage Runge–Kutta time integration is roughly 1.5 times more expensive than the single-grid iteration. The single-grid calculation using LU-SGS time integration converged in 3274 iterations. The same level of convergence can be achieved with the four-level multigrid in 950 iterations, almost halving the computational time. The four-level multigrid with the damped prolongation in Ref. 8 takes 945 iterations. Differences in convergence rate and error history between the damped prolongation in Ref. 8 and the modified damped prolongation can be hardly noticeable. The four-level multigrid using LU-SGS time integration is roughly twice more expensive than the single-grid iteration. Without damped prolongation it is impossible to obtain a multigrid solution caused by numerical instability in both the five-stage Runge–Kutta and LU-SGS schemes. Table 1 summarizes the multigrid speed-ups.

**Table 1 Comparison of convergence rate (equilibrium inviscid flow)**

| Time integration | Iteration number | Speed-up |
|---|---|---|
| Runge–Kutta 1 level | 8848 | 1.0 |
| Runge–Kutta 4 level | 710 | 7.8 |
| LU-SGS 1 level | 3274 | 1.0 |
| LU-SGS 4 level | 950 | 1.6 |
| LU-SGS 4 level[8] | 948 | 1.6 |

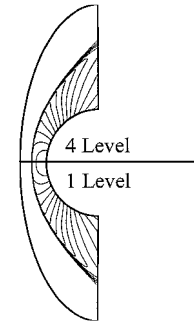


**Fig. 1a Comparison of pressure between single-grid and four-level multigrid solutions.**

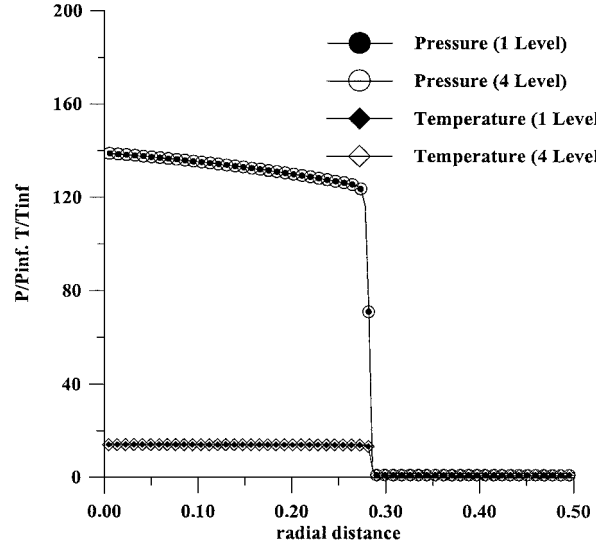


**Fig. 1b Comparison of shock profiles along the stagnation streamline between single-grid and four-level multigrid solutions.**

Comparison of convergence rate between the five-stage Runge–Kutta and the LU-SGS methods is presented in Fig. 2. Computational cost is normalized with respect to the time required to perform one iteration using single-level LU-SGS. The comparison of computational cost presents an interesting result. Computational cost using the four-level five-stage Runge–Kutta method is approximately the same as that of the single-grid LU-SGS method. This is caused by the CFL number restriction and computing time required per

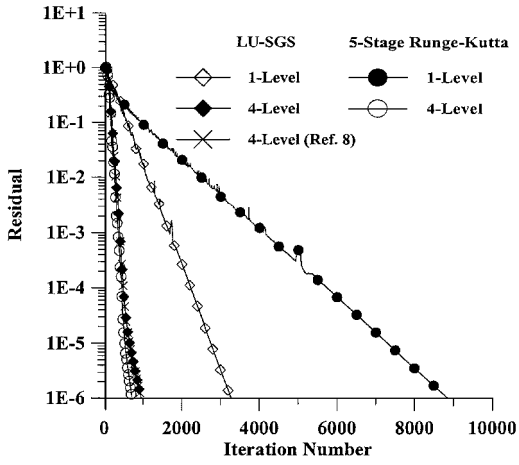


**Fig. 2a Convergence history of equilibrium inviscid flow.**

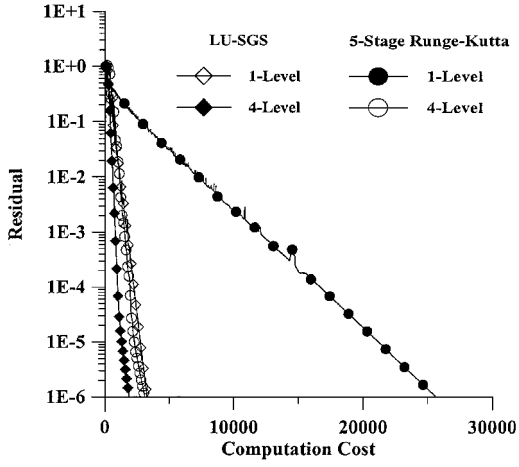


**Fig. 2b Comparison of computation cost.**

iteration. The CFL number is 1.0 when five-stage Runge–Kutta is used and 10.0 in the case of LU-SGS. Results show that the multigrid using LU-SGS method is the most efficient but slightly faster than the single-level LU-SGS or four-level five-stage Runge–Kutta methods.

**Equilibrium Viscous Flow Calculations**

Flow conditions are the same as the preceding case. The single-grid calculation using five-stage Runge–Kutta time integration converged five orders of magnitude in 9274 iterations. In this case both the implicit residual smoothing of Eqs. (23) and (27) (method 1) and the modified implicit residual smoothing of Eq. (48) (method 2) are applied to the four-level multigrid. Method 1 is not sufficient to extend local stability. Thus, $\alpha$ in the forcing term of Eq. (50) has to be reduced to the value of 0.7 to prevent a blowup, which results in the degradation of multigrid efficiency. However, this situation does not happen in method 2, and the tuning of the forcing term is not necessary. The four-level multigrid with method 1 takes 1870 iterations to achieve the same level of convergence as the single-grid calculation, which is equivalent to a 3.5 speed-up in terms of computational time. The four-level multigrid with method 2 takes 1118 iterations leading to a 6.0 speed-up in terms of computational time. The error history with five-stage Runge–Kutta time integration in Fig. 3a shows somewhat oscillatory behavior when the residual is reduced to $\mathcal{O}(10^{-4})$, which is not shown in inviscid calculation. This oscillatory behavior is caused by the error accumulated at the shock position near the far boundary, where local grids are aligned with the shock. It is local phenomenon within three or four grid points, and this error does not propagate to other domains and is quickly damped out.

The single-grid calculation using LU-SGS time integration converged five orders of magnitude in 2619 iterations. The four-level multigrid takes 480 iterations to achieve the same level of convergence, which is 2.1 times faster than the single grid calculation.

**Table 2 Comparison of convergence rate (equilibrium viscous flow)**

| Time integration | Iteration number | Speed-up |
|---|---|---|
| Runge–Kutta 1 level | 9272 | 1.0 |
| Runge–Kutta 4 level (method 1) | 1870 | 3.5 |
| Runge–Kutta 4 level (method 1) | 1118 | 6.0 |
| LU-SGS 1 level | 2619 | 1.0 |
| LU-SGS 4 level | 480 | 2.3 |

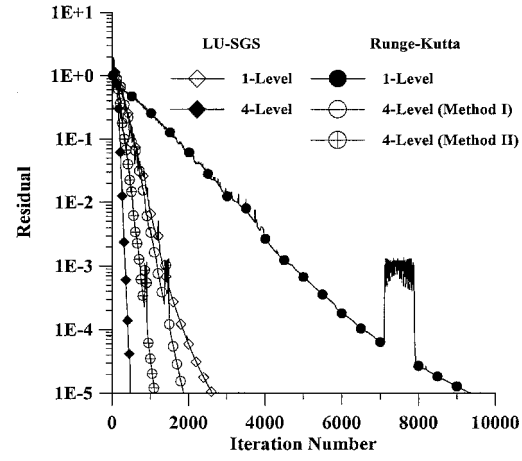


**Fig. 3a Convergence history of equilibrium viscous flow.**

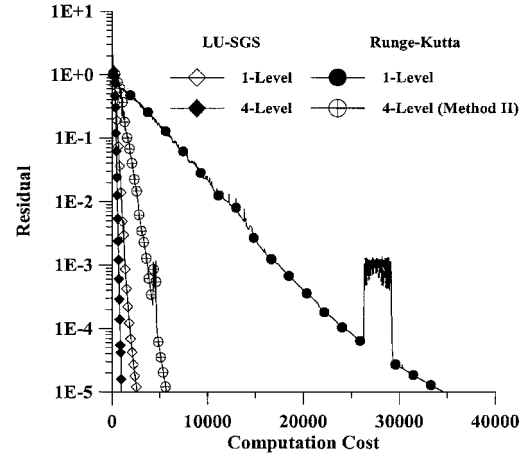


**Fig. 3b Comparison of computation cost.**

Table 2 presents the multigrid speed-ups with adopted time-integration methods. Figure 3b shows the comparison of computational cost in equilibrium viscous flows. As in the preceding case, computational cost is normalized with respect to the time required to perform one iteration using single-level LU-SGS. The computational cost of the four-level multigrid using the five-stage Runge–Kutta method is even more expensive than that of single-level LU-SGS computation, which is again caused by the CFL number restriction from the stability requirement and computing time of residuals per iteration. The CFL number is 0.7 in the case of the five-stage Runge–Kutta method and 5.0 for LU-SGS.

**Nonequilibrium Inviscid Flow Calculations**

Flow conditions correspond to a Mach number 10 flight at an altitude of 60 km. Figure 4 shows the error history of each method. The single-grid calculation with five-stage Runge–Kutta converges five orders of magnitude in 8058 iterations. The four-level multigrid takes 1192 iterations, which is approximately 4.5 times faster than the single-grid calculation in terms of computational time.

The single-grid calculation using LU-SGS time integration converges five orders of magnitude in 14,987 iterations, and it takes 2730 iterations to achieve the same level of convergence with the

**Table 3 Comparison of convergence rate (nonequilibrium inviscid flow)**

| Time integration | Iteration number | Speed-up |
|---|---|---|
| Runge–Kutta 1 level | 8,058 | 1.0 |
| Runge–Kutta 4 level | 1,192 | 4.5 |
| LU-SGS 1 level | 14,987 | 1.0 |
| LU-SGS 4 level | 2,730 | 2.7 |

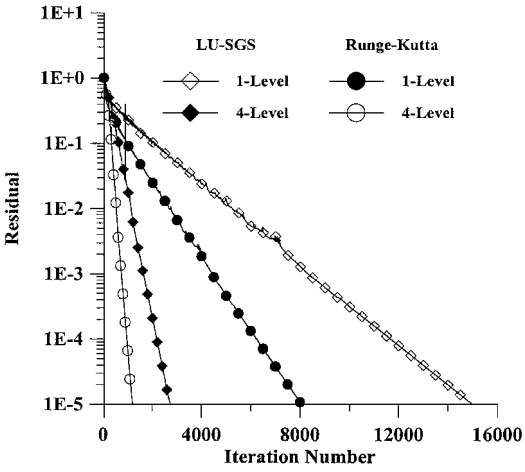


**Fig. 4a Convergence history of nonequilibrium inviscid flow.**

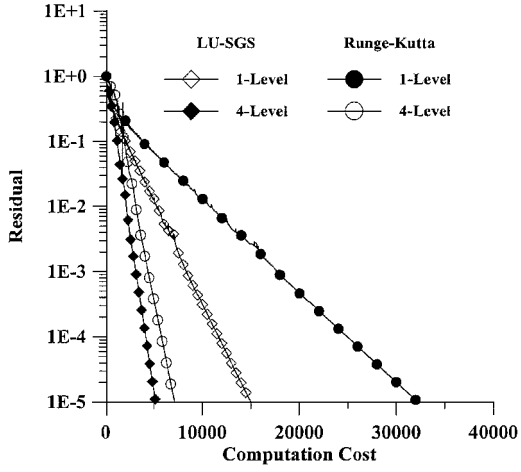


**Fig. 4b Comparison of computation cost.**

**Table 4 Comparison of convergence rate (nonequilibrium viscous flow)**

| Time integration | Iteration number | Speed-up |
|---|---|---|
| Runge–Kutta 1 level | 12,515 | 1.0 |
| Runge–Kutta 4 level (method 1) | 2,912 | 2.8 |
| Runge–Kutta 4 level (method 2) | 1,821 | 4.5 |
| LU-SGS 1 level | 26,030 | 1.0 |
| LU-SGS 4 level | 3,443 | 3.7 |

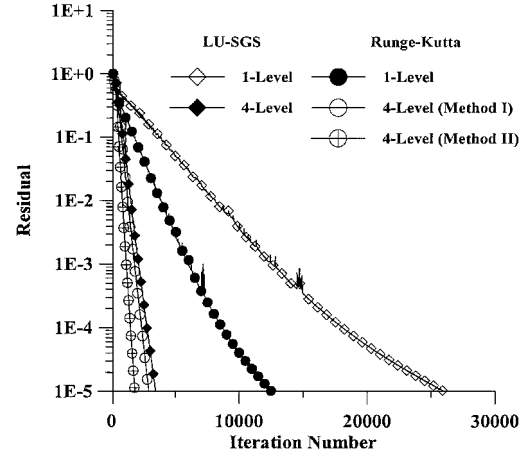


**Fig. 5a Convergence history of nonequilibrium viscous flow.**

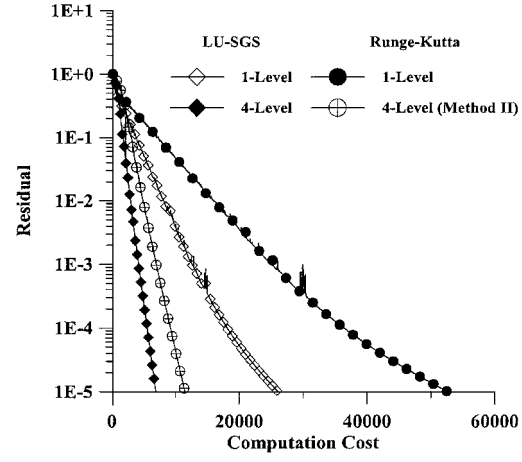


**Fig. 5b Comparison of computation cost.**

four-level multigrid. This is almost three times faster than the single-grid computation in terms of computational time. Figure 4b shows the comparison of multigrid convergence between the two multigrid smoothers, which indicates that the multigrid with LU-SGS is slightly faster than four-level five-stage Runge–Kutta. Table 3 summarizes the multigrid speed-ups.

**Nonequilibrium Viscous Flow Calculations**

Flow conditions of the first test case correspond to a Mach number 10 flight at an altitude of 60 km. Comparison between the five-stage Runge–Kutta and the LU-SGS method is presented in Fig. 5a. The single-grid calculation using five-stage Runge–Kutta time integration converges five orders of magnitude in 12,515 iterations. The four-level multigrid with the implicit residual smoothing of method 1 takes 2915 iterations to achieve the same level of convergence, which achieves approximately a 2.8 speed-up. However, $\alpha$ in the forcing term has to be down to the value of 0.7. On the other hand, the four-level multigrid with method 2 takes only 1821 iterations, which is roughly 4.5 times faster than the single-grid calculation. This shows again the efficiency and robustness of the proposed implicit residual smoothing. The single-grid calculation using LU-SGS time integration converges five orders of magnitude in 26,030 iterations. The four-level multigrid takes 3443 iterations, which is equivalent to a 3.7 speed-up compared to the single grid in terms of computation time. Figure 5b shows again that the multigrid with the LU-SGS method is more efficient than that with the five-stage Runge–Kutta method. The computation cost is normalized with respect to the time required to perform one iteration using the single-level LU-SGS time-integration method. Table 4 summarizes the multigrid speed-ups. For the study of grid refinement, three types of grids—$65 \times 169$ (grid 1), $65 \times 113$ (grid 2), $65 \times 57$ (grid 3)—are tested. In this study LU-SGS is adopted simply because of computational efficiency. Figure 6 shows the error history of each grid system, indicating the independence of the multigrid convergence rate on grid size.

The second test case involves a Mach number 15 flight at an altitude of 60 km. As in the preceding test case, LU-SGS time integration is chosen for the purpose of computational efficiency. As shown in Fig. 7a, translational and vibrational temperature distributions are compared with equilibrium temperature along the stagnation streamline. It is shown that there is a difference in shock positions between equilibrium and nonequilibrium flow. A nonequilibrium result shows the behavior of temperature relaxation right after the

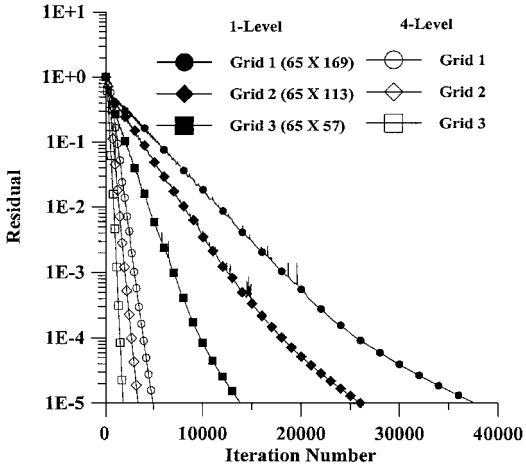


Fig. 6 Convergence history for three grid sizes.

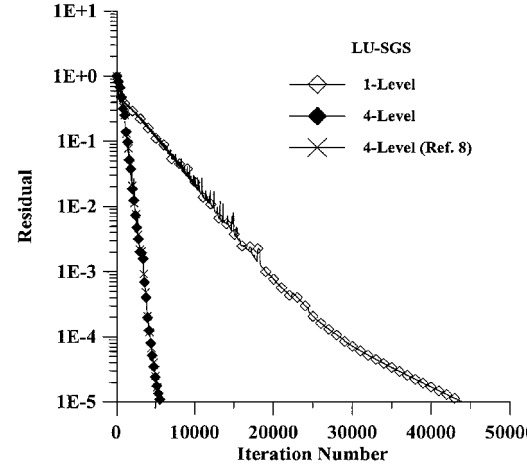


Fig. 8 Convergence history of nonequilibrium viscous flow.

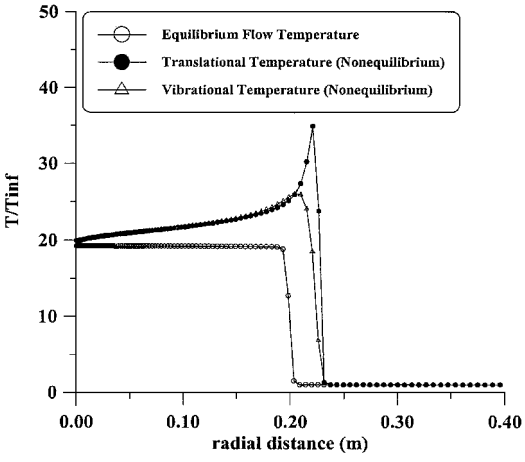


Fig. 7a Temperature distributions along the stagnation streamline.

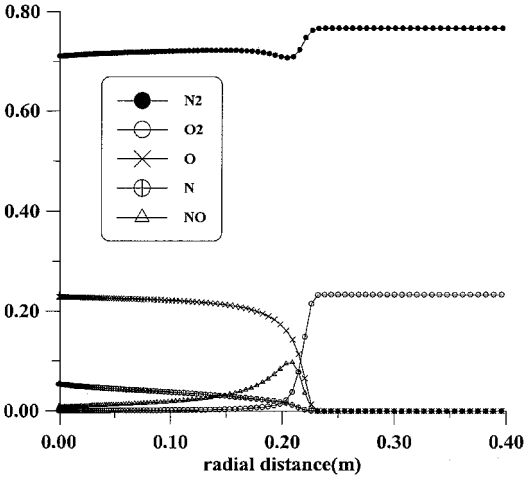


Fig. 7b Mass-fraction distributions along the stagnation streamline.

shock wave. Species mass-fraction distributions along the stagnation streamline are presented in Fig. 7b. At this flow condition the dissociation of $N_2$ is incomplete, but $O_2$ is dissociated almost completely. The mass fraction of NO increases rapidly right after the shock wave, and it slowly decreases. Figure 8 shows the error history. The single-grid calculation using LU-SGS time integration converges five orders of magnitude in 43,922 iterations. The four-level multigrid takes 5691 iterations, which is equivalent to a 3.8 speed-up in terms of computation time. The four-level multigrid with the damped prolongation in Ref. 8 takes 5695 iterations. Differences in convergence rate and error history between the damped prolongation in Ref. 8 and the modified damped prolongation in the present paper can be hardly noticeable.

## Conclusions

An efficient and robust multigrid algorithm for computations of hypersonic reacting flows has been developed. A modified damped prolongation method and modified implicit residual smoothing have been proposed and validated for test cases including equilibrium inviscid, viscous and nonequilibrium inviscid, viscous air simulations with five-species, two temperature models. Without damped prolongation multigrid solutions are not obtained as a result of severe numerical instability for all test cases, and the modified implicit residual smoothing for the explicit Runge–Kutta method does help the multigrid procedure to work very efficiently. The comparison of computation costs and multigrid speed-ups indicates that the LU-SGS method is more efficient than the five-stage Runge–Kutta time integration. Judging from the results of numerous test cases, it can be confirmed that the present methods are robust in obtaining solutions efficiently in the high-speed flow regime.

## Acknowledgments

The authors appreciate financial support by the Korea Science and Engineering Foundation (Grant 98-0200-14-01-3) and by the Brain Korea-21 Program for the Mechanical and Aerospace Engineering Research at Seoul National University.

## References

[1]Turkel, E., Swanson, R. C., Vasta, V. N., and White, J. A., "Multigrid for Hypersonic Viscous Two- and Three-Dimensional Flows," AIAA Paper 91-1572, June 1991.

[2]Koren, B., and Hemker, P. W., "Damped, Direction-Dependent Multigrid for Hypersonic Flow Computations," *Applied Numerical Mathematics*, Vol. 7, No. 4, 1991, pp. 309–328.

[3]Radespiel, R., and Swanson, R. C., "Progress with Multigrid Schemes for Hypersonic Flow Problems," *Journal of Computational Physics*, Vol. 116, No. 1, 1995, pp. 103–122.

[4]Gerlinger, P., Stoll, P., and Brüggemann, D., "An Implicit Multigrid Method for the Simulation of Chemically Reacting Flows," *Journal of Computational Physics*, Vol. 146, No. 1, 1998, pp. 322–345.

[5]Swanson, R. C., and Turkel, E., "On Central Difference and Upwind Schemes," *Journal of Computational Physics*, Vol. 101, No. 2, 1992, pp. 292–306.

[6]Gerlinger, P., and Brüggemann, D., "Multigrid Convergence Acceleration for Turbulent Supersonic Flows," *International Journal for Numerical Methods in Fluids*, Vol. 24, No. 10, 1997, pp. 1019–1035.

[7]Edwards, J. R., "An Implicit Multigrid Algorithm for Computing Hypersonic, Chemically Reacting Viscous Flows," *Journal of Computational Physics*, Vol. 123, No. 1, 1996, pp. 84–95.

[8]Zhu, Z. W., Alavilli, P., Lacor, C., and Hirch, C., "Efficiency and Robustness of Multigrid Methods for Hypersonic Flows," AIAA Paper 97-0342, Jan. 1997.

[9]Srinivassan, S., Tannehilli, J. C., and Weilmuenster, K. J., "Simplified Curve Fits for the Thermodynamic Properties of Equilibrium Air," NASA RP-1181, Aug. 1987.

[10]Gupta, R. N., Lee, K. P., Thompson, R. A., and Yos, J. M., "Calculations and Curve Fits of Thermodynamic and Transport Properties for Equilibrium Air to 30000K," NASA RP-1260, Oct. 1991.

[11]Candler, G. V., "The Computation of Weakly Ionized Hypersonic Flows in Thermo-Chemical Nonequilibrium," Ph.D. Dissertation, Dept. of Aeronautics and Astronautics, Stanford Univ., Stanford, CA, June 1988.

[12]Häuser, J., Muylaert, J., Wong, H., and Berry, W., "Computational Aerothermodynamics for 2D and 3D Space Vehicles," *Computational Methods in Hypersonic Aerodynamics*, Kluwer Academic, Norwell, MA, 1991, pp. 447–490.

[13]Park, C., *Nonequilibrium Hypersonic Aerothermodynamics*, Wiley, New York, 1990, pp. 119–170.

[14]Gupta, R. N., Yos, J. M., Thompson, R. A., and Lee, K. P., "A Review of Reaction Rates and Thermodynamic and Transport Properties for an 11-Species Air Model for Chemical and Thermal Nonequilibrium Calculations to 30,000K," NASA RP-1232, Aug. 1990.

[15]Wilke, C. R., "A Viscosity Equation for Gas Mixtures," *Journal of Chemical Physics*, Vol. 18, No. 4, 1950, pp. 517–519.

[16]Park, C., and Yoon, S., "Calculation of Real Gas Effects on Blunt-Body Trim Angles," *AIAA Journal*, Vol. 30, No. 4, 1992, pp. 999–1007.

[17]Kim, K. H., and Rho, O. H., "An Improvement of AUSM Schemes by Introducing the Pressure-based Weight Functions," *Computers and Fluids*, Vol. 27, No. 3, 1998, pp. 311–346.

[18]Liou, M. S., "A Sequel to AUSM: AUSM+," *Journal of Computational Physics*, Vol. 129, No. 2, 1996, pp. 364–382.

[19]Palmer, G., and Venkatapathy, E., "Comparison of Nonequilibrium Solution Algorithms Applied to Chemically Stiff Hypersonic Flows," *AIAA Journal*, Vol. 33, No. 7, 1995, pp. 1211–1219.

[20]Wigton, L. B., and Swanson, R. C., "Variable Coefficient Implicit Residual Smoothing," *12th International Conference on Numerical Methods in Fluid Dynamics*, Vol. 371, Lecture Notes in Physics, edited by K. W. Morton, Springer-Verlag, New York, 1990, pp. 1–11.

[21]Swanson, R. C., and Turkel, E., "Multistage Schemes with Multigrid for Euler and Navier–Stokes Equations," NASA TP 3631, Aug. 1997.

[22]Jameson, A., and Yoon, S., "Multigrid Solution of the Euler Equations Using Implicit Schemes," *AIAA Journal*, Vol. 24, No. 11, 1986, pp. 1737–1743.

T. C. Lin
*Associate Editor*